Size-Dependent Photothermal Conversion Efficiencies of Plasmonically Heated Gold Nanoparticles

ARTICLE *in* THE JOURNAL OF PHYSICAL CHEMISTRY C · DECEMBER 2013

Impact Factor: 4.77 · DOI: 10.1021/jp409067h

3 AUTHORS, INCLUDING:

Ke Jiang
University of Colorado Colorado Springs
9 PUBLICATIONS **35** CITATIONS
SEE PROFILE

Anatoliy Pinchuk
University of Colorado Colorado Springs
51 PUBLICATIONS **1,128** CITATIONS
SEE PROFILE

THE JOURNAL OF PHYSICAL CHEMISTRY C

Article

pubs.acs.org/JPCC

Size-Dependent Photothermal Conversion Efficiencies of Plasmonically Heated Gold Nanoparticles

Ke Jiang,[†] David A. Smith,[‡] and Anatoliy Pinchuk*[,†,‡]

[†]Center for Biofrontiers Institute and [‡]Department of Physics and Energy Science, University of Colorado at Colorado Springs, 1420 Austin Bluffs Pkwy, Colorado Springs, Colorado 80918, United States

Supporting Information

ABSTRACT: We report the light-to-heat energy transfer efficiencies of gold nanoparticles with variable sizes by assessing the temperature profiles of laser-activated particle suspensions in water. Gold nanoparticles with sizes ranging from 5 to 50 nm were synthesized by chemical reduction methods using sodium borohydride, sodium citrate, or hydroquinone as reducing agents. As-synthesized gold nanoparticle solution (1 mL) was loaded into a quartz cuvette and exposed to a CW green laser (532 nm). Heat input into the system by energy transfer from nanoparticles equals heat dissipation at thermal equilibrium. The transducing efficiency was then determined by plotting temperature increase as a function of laser power extinction. The efficiency increases from 0.650 ± 0.012 to 0.803 ± 0.008 as the particle size decreases from 50.09 ± 2.34 to 4.98 ± 0.59 nm, respectively. The results indicate that the photothermal properties of gold nanoparticles are size-tunable, and the variation of efficiency can be correlated to the absorption/extinction ratios calculated by Mie theory for different particle sizes. We further expanded our Mie theory calculations of absorption/extinction ratios to a broader range of diameters and wavelengths. These studies are crucial for practical applications of gold nanoparticles in nanotechnology and bioengineering, such as enhancing the treatment efficiency of laser surgery.

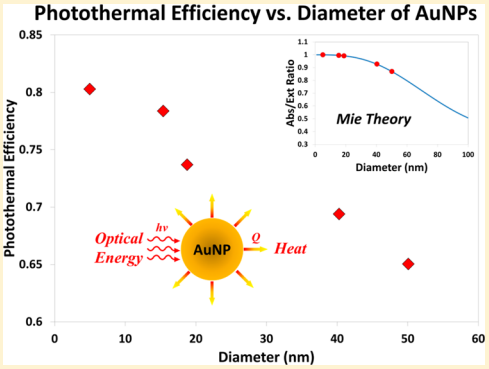

1. INTRODUCTION

A noble metal nanoparticle, such as a gold nanoparticle (AuNP) or silver nanoparticle (AgNP), displays a well-known phenomenon called surface plasmon resonance (SPR), in which the conductive free electrons collectively resonate in response to the incoming electromagnetic radiation, resulting in amplified light absorption as well as scattering. These superior optical properties have stimulated intense interest in using plasmonic nanostructures for a wide variety of biomedical applications such as bioimaging,[1−5] sensing,[6−10] medical diagnostics,[11,12] and cancer therapy.[13−16] Particularly, AuNPs and AgNPs transfer energy into heat with a high efficiency when absorbing light. During this process, the oscillating electrons transfer their kinetic energy into the particle lattice through electron−phonon interactions at a time scale of 2−5 ps, followed by phonon−phonon interactions with the surrounding medium at a time scale of 100−380 ps.[17,18] Heat dissipates through particle−medium interfaces at a rate dependent on the medium, particle size, and laser sources as the nanoparticle return to its initial temperature.[19−21] Because of the enhanced optical cross sections of metal nanoparticles as compared to their geometrical cross section,[22] the temperature around and within a single AuNP could be very high.[23,24] These photothermal effects of plasmonic nanostructures have led to the development of photothermal imaging which can reach 2.5 nanometric resolution by an optical method.[25] The unique photothermal properties have also led to the development of photothermal therapy (PTT) for cancer treatment.[26] The efficient and fast conversion of photon energy to thermal energy by direct excitation of SPR in AgNPs has enabled the fabrication of conductive silver micropatterns on an organic−inorganic hybrid film by laser-directed writing.[27]

For the purpose of illustrating photothermal properties of AuNPs from a fundamental science point of view, the temperature changes of AuNPs upon optical illumination have been investigated previously. Richardson et al. have reported the heating effect of AuNPs embedded in an ice matrix using thermooptical spectroscopy.[28] From the time-resolved Raman signals, the amount of heat generated by optically excited AuNPs was quantitatively measured. The same group later performed experimental and theoretical studies of heat transfer in an optically stimulated water droplet containing AuNPs.[29] The efficiency (η) of light-to-heat conversion was determined to be close to 1 ($0.97 < \eta < 1.03$). Chou et al. reported that the photothermal conversion efficiency of AuNPs can be turned on selectively by tuning the wavelength of the incident light to match that of the particles' SPR, and the temperature increase can be much higher when using a solid medium that is less thermal conductive than water.[30] Roper et al. have discovered that the temperature increase of colloidal

Received: September 10, 2013
Revised: December 9, 2013
Published: December 11, 2013

AuNP solutions is proportional to incident laser power and nanoparticle content at low concentrations.[17] Most recently, Freddi et al. have reported an optical method to measure the temperature of gold nanostructures by monitoring the excited state lifetime of Rhodamine B that was electrostatically bound to the gold surface.[31] However, to the best of our knowledge, the relationship between light-to-heat conversion efficiencies and the size of AuNPs has not been studied experimentally, while certain studies have shown the influence of morphology of AuNPs on their heating efficiencies.[32−34] It is then highly desirable to obtain detailed and insightful knowledge of size-dependent photothermal properties of noble metal nanoparticles for both fundamental science and practical applications in which nanoparticles are employed as light-to-heat converters.

The effectiveness of AuNPs as bioimaging contrasts and therapeutic agents strongly depends on their optical properties. Optimized photothermal treatment with AuNPs using minimal laser dosage requires high nanoparticle absorption cross sections with low scattering losses. A theoretical study using Mie theory and the discrete dipole approximation method has demonstrated that smaller nanoparticles have higher absorption/scattering ratios.[22] Accordingly, nanoparticles with smaller diameters should have higher photothermal conversion efficiencies as they would absorb more and scatter less. In this study, we investigate how the size of AuNPs in a solution affects the light-to-heat transfer efficiency. A continuous wave (CW) green laser (532 nm wavelength) was employed to activate aqueous suspensions of AuNPs loaded in a 10 mm standard cuvette. By acquiring temperature profiles of AuNP solutions, the collective energy transfer efficiencies were obtained by plotting temperature increase as a function of the extinction of incident laser power. With these energy transfer efficiencies, the temperature profiles of designated AuNP-based light-to-heat converters can be predicted and/or optimized. We have also extended our study to a broader theoretical calculation in which the absorption/extinction ratios of AuNP with different diameters for varying wavelengths were obtained by Mie theory.

2. EXPERIMENTAL METHODS AND MATERIALS

2.1. Synthesis of AuNPs. In this study, AuNPs of sizes ranging from approximately 5 to 50 nm were prepared by chemical reduction methods using different growth methods and reducing agents. (1) For AuNPs with sizes of about 5 nm, 100 mL of $HAuCl_4$ (Acros Organics, ≥49.0% Au) aqueous solution (0.2 mM) was mixed with 200 μL of 0.1 M trisodium citrate (NaCit) (Fisher Scientific, 99.0%) solution under stirring in an ice bath. 3 mL of freshly prepared $NaBH_4$ (Acros Organics, 98.0%) solution (0.1 M) was added into the above mixture dropwise. The color of the solution changed to orange, indicating the formation of AuNPs. The AuNP solution was then kept in the ice bath under vigorous stirring for another 10 min. (2) AuNPs with sizes of 15−40 nm were prepared by a trisodium citrate (NaCit) reduction method. Briefly, a designated amount of NaCit (Fisher Chemical) aqueous solution (0.1 M) was added into 100 mL of boiling $HAuCl_4$ solution (0.2 mM). The molar ratio of NaCit to $HAuCl_4$ was varied as 0.9, 2, and 2.5 to obtain AuNPs with sizes of about 40, 20, and 15 nm, respectively. After the color of the solution turned from pale yellow to burgundy, the solution was kept boiling for another 5 min before cooling to room temperature. (3) AuNPs with bigger sizes were prepared according to a seeding method reported previously.[35] First, a AuNP seed solution was prepared by the sodium citrate reduction method described above with a molar ratio of NaCit to $HAuCl_4$ as 4:1. Then, 100 μL of AuNP seed solution was added into 10 mL of aqueous solution containing 0.2 mM of $HAuCl_4$ and 1 mM of trisodium citrate, followed by the addition of 100 μL of 30 mM hydroquinone solution (Acros Organics, 99.5%). All of the as-prepared AuNP solutions were directly used for the temperature profile measurements without further purification.

2.2. Modeling. A collective heating model based on previously literature[17,29] is employed to describe the temperature profiles of AuNP solutions. The change in thermal energy of a solution is determined by the rate of heat input from the laser via the AuNPs (Q_{in}) and the rate of heat dissipation to the external environment (Q_{out}), which can be expressed as[17,29]

$$\sum_i m_i C_i \frac{dT}{dt} = Q_{in} - Q_{out} \quad (1)$$

where m_i and C_i are the mass and specific heat capacity of component i, respectively. T is the temperature, and t is time. In the AuNP solutions considered here, the mass of AuNPs is significantly less than that of water, and the heat capacity of gold (0.129 J g^{-1} K^{-1}) is also much smaller than that of water (4.18 J g^{-1} K^{-1}). Hence, the thermal energy of the AuNPs is negligible, and eq 1 is simplified as

$$m_w C_w \frac{dT}{dt} = Q_{in} - Q_{out} \quad (2)$$

where m_w and C_w are the mass and specific heat capacity of water, respectively.

The rate of heat produced by AuNPs upon laser exposure can be expressed as[17,29]

$$Q_{in} = (I_0 - I_{tr})\eta \quad (3)$$

where I_0 is the incident laser power (~228 mW), I_{tr} is the power of laser that is transmitted through the solution, and η is the light-to-heat conversion efficiency.

The heat dissipated to the external environment is given by[17,29]

$$Q_{out} = \sum hS[T(t) - T_0] \quad (4)$$

where h is the heat transfer efficiency, S is the surface area of the interface between the AuNP solution and external environment, $T(t)$ is the temperature at time t, and T_0 is the ambient room temperature. By defining $\Delta T \equiv T(t) - T_0$, eq 2 can be expressed as

$$\frac{d\Delta T}{dt} = \frac{(I_0 - I_{tr})\eta}{m_w C_w} - \frac{\sum hS}{m_w C_w}\Delta T \quad (5)$$

From here, we would define $B \equiv \sum hS/m_w C_w$ as the constant rate of heat dissipation from the AuNP solution to the external environment, which can be determined by measuring the decreasing temperature profile after laser is turned off. The temperature trace in this regime can be found by setting $(I_0 - I_{tr}) = 0$ in eq 5 and solving for $T(t)$ using the limit $T(0) = T_m$. The result is

$$T(t) = T_0 + (T_m - T_0)\exp(-Bt) \quad (6)$$

where T_m is the maximum temperature at which the laser is turned off.

dx.doi.org/10.1021/jp409067h | J. Phys. Chem. C 2013, 117, 27073−27080

At thermal equilibrium, where Q_{in} equals Q_{out}, the temperature will remain constant. This gives (by setting eq 5 equal to zero)

$$\frac{(I_0 - I_{tr})\eta}{m_w C_w B} = \Delta T \quad (7)$$

The significance of eq 7 is that if the mass of the solution was kept constant for each measurement, and B was calculated by a data fit to eq 6, then η could be determined by plotting the temperature increase as a function of extinct laser power. Finally, by solving eq 5 for $T(t)$, using the limit $T(0) = T_0$, we can get the temperature profile when the laser is on:

$$T(t) = T_0 + \frac{(I_0 - I_{tr})\eta}{m_w C_w B}[1 - \exp(-Bt)] \quad (8)$$

2.3. Temperature Profile Measurements. The temperature profiles were obtained via a thermocouple inserted into 1 mL AuNP solution that was loaded into a standard 10 mm quartz cuvette, as shown in Figure 1. The solution was kept stirring to achieve uniform temperature distribution upon laser activation. A CW green laser (532 nm, ~228 mW) with illumination area of about 2 mm in diameter was used to illuminate the AuNP solution. A control experiment with pure water loaded in the cuvette showed that the applied laser energy does not induce a detectable temperature increase in the water. Hence, the temperature increase with the presence of AuNPs is exclusively attributed to heat transduced from the light by AuNPs. Because of the fluctuation of laser powers, the power of the incident and transmitted laser was measured by a luminometer during each temperature profile measurement. In addition, these values were further corrected by taking into account of the loss of transmission at the solid–liquid and solid–air interfaces. In other words, the variation of laser power when transmitting through the cuvette loaded with pure water was measured and subtracted from the value of $(I_0 - I_{tr})$ for each sample.

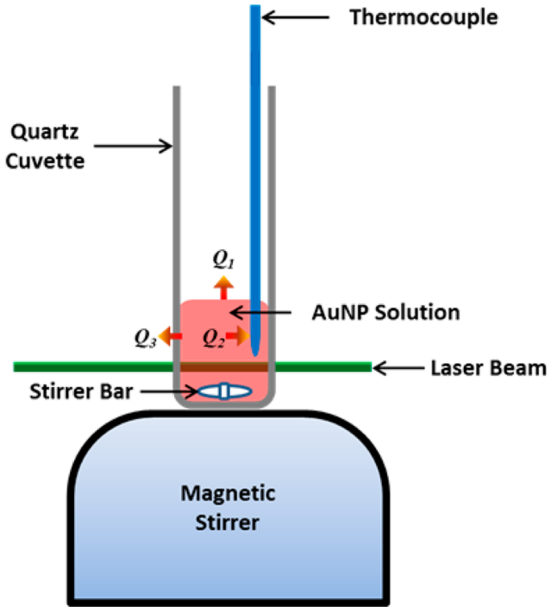

Figure 1. Experimental setup for measuring the temperature profile of AuNP solutions. Q_1, Q_2, and Q_3 represent the heat dissipation through water–air, water–thermocouple, and water–cuvette interfaces, respectively.

2.4. Instrumentation. The extinction spectra of AuNP solutions were measured by a UV–vis spectrometer (Lambda 1050, PerkinElmer). The sizes of AuNPs were determined by a cold field emission scanning electron microscope (FE SEM) (Hitachi, S-5000H) operated at 5 kV. Before SEM characterization, the AuNP samples were purified by centrifuging and redispersing thrice to remove unreacted precursors. The particle sizes were then analyzed using SEM images by ImageJ. The CW green laser was generated by a Verdi-V5, Coherent. The laser power was measured by a luminometer (PowerMax PS10Q, Coherent).

3. RESULTS AND DISCUSSION

3.1. Characterization of AuNPs. In this study, AuNPs with small, medium, and large diameters were synthesized by a wet-chemistry route using sodium borohydride, sodium citrate, or hydroquinone as the reducing agent, respectively. The average diameters of as-synthesized AuNPs are approximately 5, 15, 20, 40, and 50 nm. For the purpose of performing statistical analysis, three AuNP samples were prepared for each specific size range. Figure 2a–e shows representative SEM images of five AuNP samples with different diameters. The SEM images and histograms of particle size for the other ten samples are shown in Figure S1 (Supporting Information). The average particle diameter and standard deviation were then calculated from the values of three independent samples and shown in Table 1. From SEM images, it can be seen that the as-prepared AuNPs are spherical in shape. It is well-known that the morphology of AuNPs would affect the rate of heat generation.[32] Generally, rod-shaped nanoparticles have higher heat generation rate as compared to spherical shape when the volume of the particle is the same.[33] In this study, we focused on spherical-shaped nanoparticles and investigate the size dependence of collective photothermal efficiencies. The extinction spectra of as-prepared colloidal AuNP solutions (Figure 2f) exhibit characteristic SPR extinction of AuNPs and the red-shift of SPR wavelength as the particle size increases, which are consistent with those reported in the literature.[36,37]

3.2. Temperature Profiles of AuNP Solutions and Determination of Heat Dissipation Constant. For the temperature profile measurements, as-prepared AuNP solutions were further diluted by a factor of 1.3, 2, 4, and 10. A series of dilutions would lead to varying extinction of laser power and the subsequent temperature increases, thereby increasing the accuracy of photothermal efficiency determination based on eq 7. Figure 3a shows typical temperature profiles of colloidal AuNP solutions with different particle sizes at the original concentration (approximately 0.2 mM according to the concentration of precursor gold ions). The temperature of the AuNP solution increased exponentially upon laser illumination, reached the equilibrium after ~1200 s, and then returned to the ambient value after discontinuing irradiation. It is noteworthy that a less volume of the AuNP solution would give rise to a faster rate of reaching temperature equilibrium, which was evidenced by previous reports.[17,29] Typical temperature increase profiles of AuNP solutions with different concentrations are shown in Figure S2 (Supporting Information).

According to eq 7, the heat dissipation rate constant (B) must be determined before evaluating the photothermal efficiency. Using eq 6, its value can be calculated by the slope

dx.doi.org/10.1021/jp409067h | J. Phys. Chem. C 2013, 117, 27073–27080

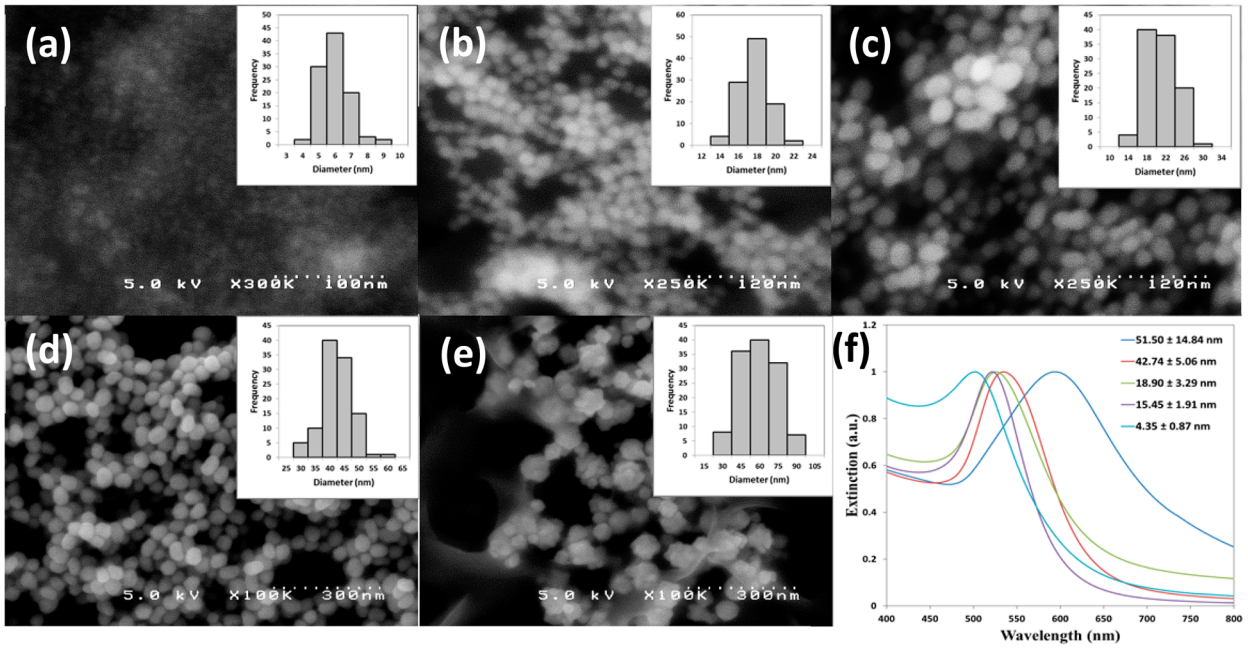

Figure 2. SEM images of AuNPs with diameter of (a) 4.35 ± 0.87, (b) 15.45 ± 1.91, (c) 18.90 ± 3.29, (d) 42.74 ± 5.06, and (e) 51.50 ± 14.84 nm. Insets in (a–e) show the histogram of size distribution of each sample. (f) UV–vis extinction spectra of AuNPs with different diameters.

Table 1. Light-to-Heat Energy Conversion Efficiencies and Absorption/Extinction Ratios of AuNPs with Different Diameters

diam[a] (nm)	conv efficiency[a] (η)	abs/ext ratio[b] (@diameter)
4.98 ± 0.59	0.803 ± 0.008	0.999 (@5 nm)
15.38 ± 1.29	0.784 ± 0.008	0.996 (@15 nm)
18.77 ± 0.77	0.737 ± 0.021	0.992 (@19 nm)
40.29 ± 2.28	0.694 ± 0.005	0.928 (@40 nm)
50.09 ± 2.34	0.650 ± 0.012	0.869 (@50 nm)

[a]Experimental results obtained from three independent samples at each particle size range. [b]Theoretical calculations based on Mie theory. Each number is corresponded to a specific diameter shown at the right.

of temperature decay profiles after the laser is turned off. Figure 3b shows the plot of the natural log of $(T(t) - T_0)/(T_m - T_0)$ as a function of time after the laser was turned off. The linear relationship indicates that a first-order decay is observed as the temperature drops back to the temperature of the external environment. In addition, it can be seen that the heat dissipation rate is independent of the size of AuNPs with negligible variations. To further confirm that the value of heat dissipation rate is constant, we inspected the possible routes by which the AuNP solution would dissipate heat into the external environment. In our experimental setup, the heat dissipation involves conduction through three interfaces: (1) the water–air interface (Q_1), (2) the water–thermocouple interface (Q_2), and

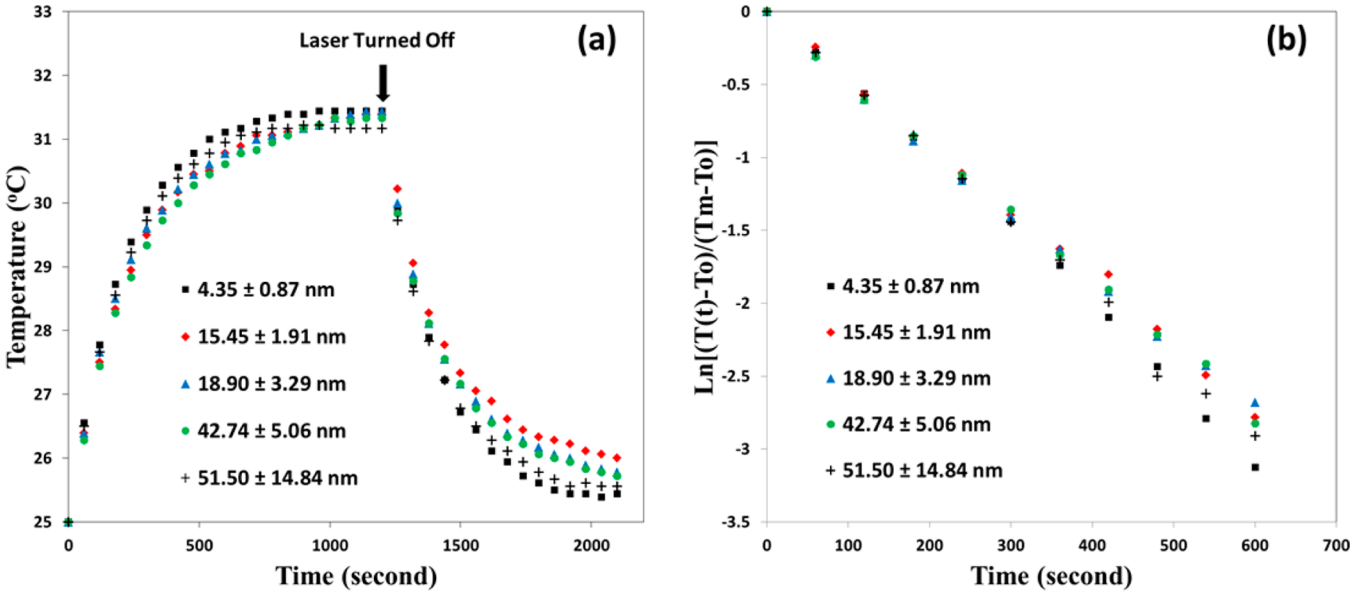

Figure 3. (a) Temperature profiles of AuNP solutions with different particle sizes and equal approximate concentrations of 0.2 mM. (b) Plots of the natural log of $(T(t) - T_0)/(T_m - T_0)$ as a function of time after the laser was turned off.

dx.doi.org/10.1021/jp409067h | J. Phys. Chem. C 2013, 117, 27073–27080

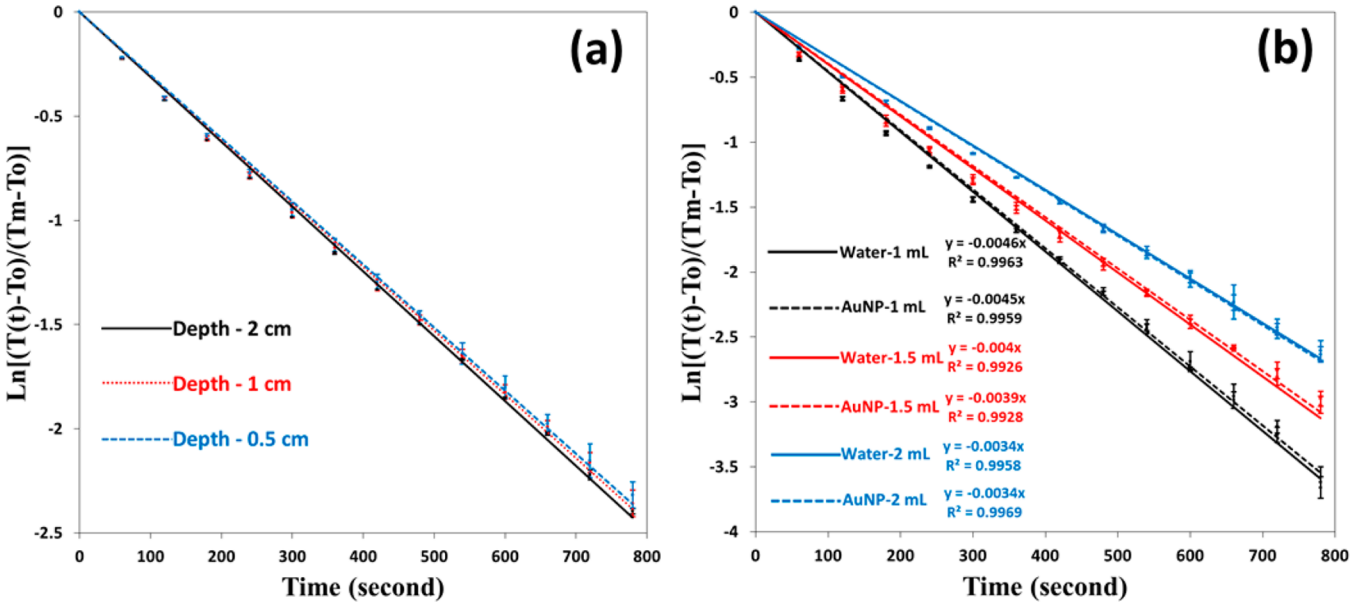

Figure 4. Plots of the natural log of $(T(t) - T_0)/(T_m - T_0)$ versus time for (a) different insertion depths of the thermocouple into the AuNP solution and (b) different volumes of solutions loaded into the cuvette.

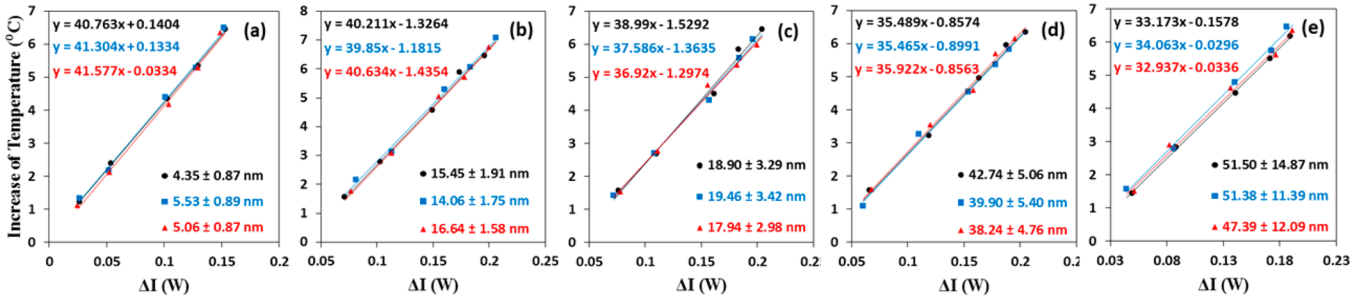

Figure 5. Temperature increases of AuNP solutions as a function of the laser power extinction by AuNPs with average diameters of (a) 4.98 ± 0.59, (b) 15.38 ± 1.29, (c) 18.77 ± 0.77, (d) 40.29 ± 2.28, and (e) 50.09 ± 2.34 nm.

(3) the water−cuvette interface (Q_3), as shown in Figure 1. Obviously, the area of the water−air interface is constant, while those of the water−thermocouple and water−cuvette interfaces are adjustable. For the purpose of understanding which route dominates the overall heat dissipation, two control experiments were conducted. In the first experiment, the depth of the thermocouple inserted into the solution was changed, resulting in a change of water−thermocouple interface area. As shown in Figure 4a, the different insertion depths did not cause significant change to the overall dissipation rate, indicating that the heat dissipation through the water−thermocouple interface is negligible. In the second experiment, different volumes of AuNP solutions, as well as pure water, were heated up to an elevated temperature using a hot plate before measuring the temperature decay profile. As shown in Figure 4b, the heat dissipation rate is mainly related to the volume of solution loaded into the cuvette, and the presence of AuNPs in the water does not significantly affect the heat dissipation rate. Consequently, since the experimental setup was always kept the same (1 mL of AuNP solution loaded into the cuvette), the heat dissipation rate constant (B) should be identical regardless of AuNP size. An average value of B was then calculated to be $(4.66 \pm 0.31) \times 10^{-3}$ s^{-1} based on the slopes of the best-fit lines from the data shown in both Figure 3b and Figure 4b.

3.3. Photothermal Efficiency and Mie Theory Calculation. Based on eq 7, the total temperature rise with laser illumination is proportional to the extinction of laser power by the AuNP solution. Consequently, the heat conversion efficiency η can be determined from the plot of ΔT as a function of laser power extinction. As shown in Figure 5, it can be clearly seen that there is a linear relationship between temperature increase and laser power extinction, indicating that the energy conversion efficiency η represents an intrinsic property of AuNPs. The values of η were calculated for each sample using the slopes of fitted linear lines. The average and standard deviation are shown in Table 1. It is clear that photothermal efficiency η increases as the diameter of AuNPs decreases. According to Mie theory, larger nanoparticles have more scattering than absorption. Hence, the observed decrease of photothermal efficiency was attributed primarily to the enhanced scattering as the particle size increases. We then calculated the absorption/extinction (abs/ext) ratios of AuNPs in water with different diameters at the 532 nm wavelength using Mie theory.[38] The theoretical abs/ext ratios corresponding to each experimental particle size are shown in Table 1 (right column). Intuitively, it makes sense that the conversion efficiency η would be proportional to the abs/ext ratio in order to account for scattered light which removes nonheat energy from the system. We further plotted the photothermal

dx.doi.org/10.1021/jp409067h | J. Phys. Chem. C 2013, 117, 27073−27080

efficiencies obtained experimentally as a function of AuNP diameters, along with the theoretically calculated abs/ext ratios of AuNPs with different diameters at the wavelength 532 nm. As shown in Figure 6, it can be seen that the photothermal

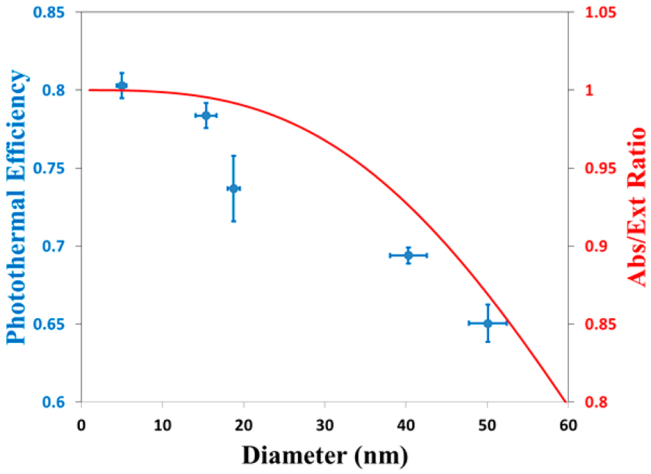

Figure 6. Change of photothermal efficiency as a function of AuNP diameters. The experimental data were presented (as blue color) with standard deviations for both diameters and efficiencies. The red curve represents theoretical abs/ext ratios for AuNPs with varying diameters at the wavelength 532 nm calculated by the Mie theory.

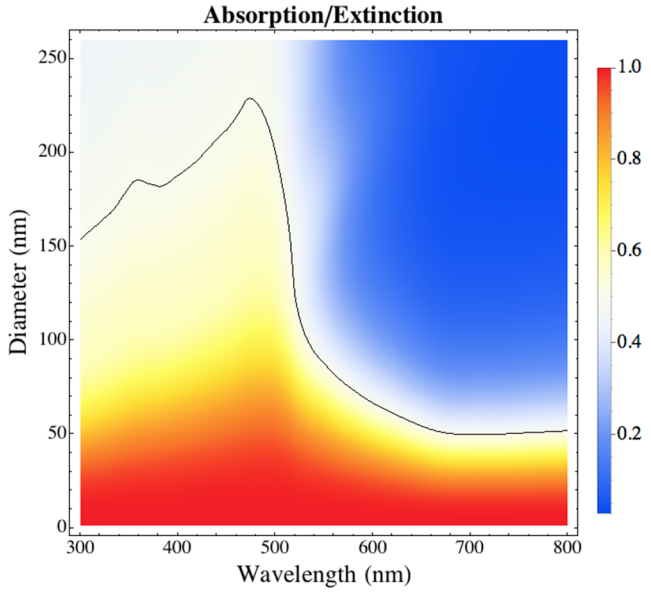

Figure 7. Intensity plot illustrating Mie theory values of absorption/extinction as a function of diameter and wavelength for gold nanospheres in water. The black curve represents the points where absorption/extinction = 1/2 (i.e., where absorption = scattering).

efficiency decreased to a comparable magnitude as the abs/ext ratio decreased, noting that the primary *y*-axis (on the left) has the same scale as that of the secondary *y*-axis (on the right). Although our experimental data cannot be quantitatively correlated with theoretical results, they do allow us to make some general conclusions about the important role of particle sizes in determining the collective photothermal efficiency of AuNPs. Other possible contributions to the collective heating effects of AuNPs may include the varying heat generation[23] and dissipation rate[19] on a single particle level due to the different surface-to-volume ratios. The thermal conductivity and viscosity of the matrix, such as water or polymeric gels, may also affect the overall heating effects of suspended AuNPs.[30] Additional comprehensive studies into these effects may provide further details on the heating process.

Finally, since the abs/ext ratios play a key role in determining the value of η, we further expanded our Mie theory calculations of abs/ext to a broader range of diameters and wavelengths. All of our Mie theory calculations used the gold optical constants from Johnson and Christy,[39] and a constant value of 1.33 was used as the index of refraction of water. Figure 7 is an intensity plot which illustrates the basic trend of higher abs/ext values for smaller AuNPs in the entire spectral range of 300−800 nm. These results indicate that AuNPs with smaller sizes should transduce energy from light to heat more efficiently than larger nanoparticles. It is noteworthy to point out that at the single particle level a larger nanoparticle would generate more heat due to its higher surface area. However, the photothermal efficiency investigated in our experiment is a collective effect of many AuNPs suspended in a solvent. Therefore, it could serve as a measurement of how efficiently the AuNP suspension could transduce the absorbed optical energy into heat. In this context, the data presented in Figure 7 will become highly valuable as it could provide a reference which illustrates how the particle size influences the temperature change of a nanoparticle suspension using selected laser source. Although it will remain as a challenging task to establish precisely a quantitative correlation between theoretical abs/ext ratios and practical temperature changes, our study explicitly illustrated the qualitative correlations between abs/ext ratios and collective photothermal efficiencies of AuNPs.

4. CONCLUSION

In this study, the photothermal properties of AuNPs with various sizes were investigated. The collective heating effect of AuNP solutions was assessed by activating the solutions with a CW green laser. After obtaining the heat dissipation rate constant by measuring the temperature decay of AuNP solutions, the energy transfer efficiency was evaluated by plotting temperature increase as a function of laser power extinction. The results show that the light-to-heat energy conversion efficiency is size-tunable in that smaller nanoparticles possess higher efficiencies due to higher abs/ext ratios. A qualitative correlation between experimental photothermal efficiency and theoretical abs/ext ratio was established successfully. We further extended the Mie theory calculation to a broader range of particle sizes and optical wavelengths, providing a reference that might be used to quantitatively investigate the heating process of colloidal AuNPs. These results have significant scientific merits for optimizing AuNP-based light-to-heat conversion systems, including promising surgical applications with laser scalpels.

■ ASSOCIATED CONTENT

Supporting Information

SEM images of other 10 AuNP samples that were not presented in the main text (Figure S1) and temperature profiles of aqueous suspension of AuNPs with different concentrations and diameters (Figure S2). This material is available free of charge via the Internet at http://pubs.acs.org.

AUTHOR INFORMATION

Corresponding Author

*Fax 719-255-3013; Ph 719-255-3556; e-mail apinchuk@uccs.edu (A.P.).

Notes

The authors declare no competing financial interest.

ACKNOWLEDGMENTS

This work is supported by funding from The Center for Biofrontiers Institute, University of Colorado at Colorado Springs. We acknowledge the Characterization Center for Materials & Biology in the University of Texas at Arlington for SEM characterization.

REFERENCES

(1) Sokolov, K.; Follen, M.; Aaron, J.; Pavlova, I.; Malpica, A.; Lotan, R.; Richards-Kortum, R. Real-Time Vital Optical Imaging of Precancer Using Anti-Epidermal Growth Factor Receptor Antibodies Conjugated to Gold Nanoparticles. *Cancer Res.* **2003**, *63*, 1999−2004.

(2) El-Sayed, I. H.; Huang, X.; El-Sayed, M. A. Surface Plasmon Resonance Scattering and Absorption of Anti-EGFR Antibody Conjugated Gold Nanoparticles in Cancer Diagnostics: Applications in Oral Cancer. *Nano Lett.* **2005**, *5*, 829−834.

(3) Shi, X.; Wang, S.; Meshinchi, S.; Antwerp, M. E. V.; Bi, X.; Lee, I.; Baker, J. R., Jr. Dendrimer-Entrapped Gold Nanoparticles as a Platform for Cancer-Cell Targeting and Imaging. *Small* **2007**, *3*, 1245−1252.

(4) Popovtzer, R.; Agrawal, A.; Kotov, N. A.; Popovtzer, A.; Balter, J.; Carey, T. E.; Kopelman, R. Targeted Gold Nanoparticles Enable Molecular CT Imaging of Cancer. *Nano Lett.* **2008**, *8*, 4593−4596.

(5) Kim, D.; Park, S.; Lee, J. H.; Jeong, Y. Y.; Jon, S. Antibiofouling Polymer-Coated Gold Nanoparticles as a Contrast Agent for in Vivo X-ray Computed Tomography Imaging. *J. Am. Chem. Soc.* **2007**, *129*, 7661−7665.

(6) Elghanian, R.; Storhoff, J. J.; Mucic, R. C.; Letsinger, R. L.; Mirkin, C. A. Selective Colorimetric Detection of Polynucleotides Based on the Distance-Dependent Optical Properties of Gold Nanoparticles. *Science* **1997**, *277*, 1078−1080.

(7) Liu, J.; Lu, Y. A Colorimetric Lead Biosensor Using DNAzyme-Directed Assembly of Gold Nanoparticles. *J. Am. Chem. Soc.* **2003**, *125*, 6642−6643.

(8) Choi, Y.; Ho, N.-H.; Tung, C.-H. Sensing Phosphatase Activity by Using Gold Nanoparticles. *Angew. Chem., Int. Ed.* **2007**, *46*, 707−709.

(9) Liu, J.; Lu, Y. Fast Colorimetric Sensing of Adenosine and Cocaine Based on a General Sensor Design Involving Aptamers and Nanoparticles. *Angew. Chem.* **2006**, *118*, 96−100.

(10) Saha, K.; Agasti, S. S.; Kim, C.; Li, X.; Rotello, V. M. Gold Nanoparticles in Chemical and Biological Sensing. *Chem. Rev.* **2012**, *112*, 2739−2779.

(11) Ray, P. C. Diagnostics of Single Base-Mismatch DNA Hybridization on Gold Nanoparticles by Using the Hyper-Rayleigh Scattering Technique. *Angew. Chem., Int. Ed.* **2006**, *45*, 1151−1154.

(12) Rosi, N.; Mirkin, C. A. Nanostructures in Biodiagnostics. *Chem. Rev.* **2005**, *105*, 1547−1562.

(13) Hirsch, L. R.; Stafford, R. J.; Bankson, J. A.; Sershen, S. R.; Rivera, B.; Price, R. E.; Hazle, J. D.; Halas, N. J.; West, J. L. Nanoshell-Mediated Tumor Ablation Using near Infrared Light under Magnetic Resonance Guidance. *Proc. Natl. Acad. Sci. U. S. A.* **2003**, *100*, 13549−13554.

(14) O'Neal, D. P.; Hirsch, L. R.; Halas, N. J.; Payne, J. D.; West, J. L. Photo-thermal Tumor Ablation in Mice Using near Infrared-Absorbing Nanoparticles. *Cancer Lett.* **2004**, *209*, 171−176.

(15) Loo, C.; Lowery, A.; Halas, A.; West, N.; Drezek, J.; Immunotargeted, R. Nanoshells for Integrated Cancer Imaging and Therapy. *Nano Lett.* **2005**, *5*, 709−711.

(16) Huang, X.; El-Sayed, I. H.; Qian, W.; El-Sayed, M. A. Cancer Cell Imaging and Photothermal Therapy in the Near-Infrared Region by Using Gold Nanorods. *J. Am. Chem. Soc.* **2006**, *128*, 2115−2120.

(17) Roper, D. K.; Ahn, W.; Hoepfner, M. Microscale Heat Transfer Transduced by Surface Plasmon Resonant Gold Nanoparticles. *J. Phys. Chem. C* **2007**, *111*, 3636−3641.

(18) Rashidi-Huyeh, M.; Palpant, B. Thermal Response of Nanocomposite Materials under Pulsed Laser Excitation. *J. Appl. Phys.* **2004**, *96*, 4475−4482.

(19) Hu, M.; Hartland, G. V. Heat Dissipation for Au Particles in Aqueous Solutions: Relaxation Time versus Size. *J. Phys. Chem. B* **2002**, *106*, 7029−7033.

(20) Plech, A.; Kotaidis, V.; Grésillon, S.; Dahmen, C.; von Plessen, G. Laser-Induced Heating and Melting of Gold Nanoparticles Studied by Time-Resolved X-ray Scattering. *Phys. Rev. B* **2004**, *70*, 195423.

(21) Wilson, O. M.; Hu, X.; Cahill, D. G.; Braun, P. V. Colloidal Metal Particles as Probes of Nanoscale Thermal Transport in Fluids. *Phys. Rev. B* **2002**, *66*, 224301.

(22) Jain, P. K.; Lee, K. S.; El-Sayed, I. H.; El-Sayed, M. A. Calculated Absorption and Scattering Properties of Gold Nanoparticles of Different Size, Shape, and Composition: Applications in Biological Imaging and Biomedicine. *J. Phys. Chem. B* **2006**, *110*, 7238−7248.

(23) Pustovalov, V. K. Theoretical Study of Heating of Spherical Nanoparticle in Media by Short Laser Pulses. *Chem. Phys.* **2005**, *308*, 103−108.

(24) Zeng, N.; Murphy, A. B. Heat Generation by Optically and Thermally Interacting Aggregates of Gold Nanoparticles Under Illumination. *Nanotechnology* **2009**, *20*, 375702.

(25) Boyer, D.; Tamarat, P.; Maali, A.; Lounis, B.; Orrit, M. Photothermal Imaging of Nanometer-Sized Metal Particles among Scatterers. *Science* **2002**, *297*, 1160−1163.

(26) Pissuwan, D.; Valenzuela, S. M.; Cortie, M. B. Therapeutic Possibilities of Plasmonically Heated Gold Nanoparticles. *Trends Biotechnol.* **2006**, *24*, 62−67.

(27) Aminuzzaman, M.; Watanabe, A.; Miyashita, T. Fabrication of Conductive Silver Micropatterns on an Organic-Inorganic Hybrid Films by Laser Direct Writing. *Thin Solid Films* **2009**, *517*, 5935−5939.

(28) Richardson, H. H.; Hickman, Z. N.; Govorov, A. O.; Thomas, A. C.; Zhang, W.; Kordesch, M. E. Thermooptical Properties of Gold Nanoparticles Embebbed in Ice: Characterization of Heat Generation and Melting. *Nano Lett.* **2006**, *6*, 783−788.

(29) Richardson, H. H.; Carlson, M. T.; Tandler, P. J.; Hernandez, P.; Govorov, A. O. Experimental and Theoretical Studies of Light-to-Heat Conversion and Collective Heating Effects in Metal Nanoparticle Solutions. *Nano Lett.* **2009**, *9*, 1139−1146.

(30) Chou, C.-H.; Chen, C.-D.; Wang, C. R. C. Highly Efficient, Wavelength-Tunable, Gold Nanoparticle Based Optothermal Nanoconvertors. *J. Phys. Chem. B* **2005**, *109*, 11135−11138.

(31) Freddi, S.; Sironi, L.; D'Antuono, R.; Morone, D.; Donà, A.; Cabrini, E.; D'Alfonso, L.; Collini, M.; Pallavicini, P.; Baldi, G.; Maggioni, D.; Chirico, G. A Molecular Thermometer for Nanoparticles for Optical Hyperthermia. *Nano Lett.* **2013**, *13*, 2004−2010.

(32) Baffou, G.; Quidant, R.; García de Abajo, F. J. Nanoscale Control of Optical Heating in Complex Plasmonic Systems. *ACS Nano* **2010**, *4*, 709−716.

(33) Baffou, G.; Quidant, R.; Girard, C. Heat Generation in Plasmonic Nanostructures: Influence of Morphology. *Appl. Phys. Lett.* **2009**, *94*, 153109.

(34) Pallavicini, P.; Dona, A.; Casu, A.; Chirico, G.; Collini, M.; Dacarro, G.; Falqui, A.; Milanese, C.; Sironi, L.; Taglietti, A. Triton X-100 for Three-Plasmon Gold Nanostars with Two Photothermally Active NIR (Near IR) and SWIR (Short-Wavelength IR) Channels. *Chem. Commun.* **2013**, *49*, 6265−6267.

(35) Perrault, S. D.; Chan, W. C. W. Synthesis and Surface Modification of Highly Monodispersed, Spherical Gold Nanoparticles of 50−200 nm. *J. Am. Chem. Soc.* **2009**, *131*, 17042−17043.

(36) Njoki, P. N.; Lim, I-I. S.; Mott, D.; Park, H. Y.; Khan, B.; Mishra, S.; Sujakumar, R.; Luo, J.; Zhong, C.-J. Size Correlation of

Optical and Spectroscopic Properties for Gold Nanoparticles. *J. Phys. Chem. C* **2007**, *111*, 14664−14669.
(37) Link, S.; El-Sayed, M. A. Size and Temperature Dependence of the Plasmon Absorption of Colloidal Gold Nanoparticles. *J. Phys. Chem. B* **1999**, *103*, 4212−4217.
(38) Bohren, C.; Huffman, D. *Absorption and Scattering by a Sphere. Absorption and Scattering of Light by Small Particles*; Wiley-VCH Verlag GmbH: Weinheim: 1983; pp 82−129.
(39) Johnson, P. B.; Christy, R. W. Optical Constants of the Noble Metals. *Phys. Rev. B* **1972**, *6*, 4370−4379.